Earthquake extraction and correlation energy at Long Beach, California seismic survey

Jason P. Chang and Sjoerd de Ridder

ABSTRACT

Seismic interferometry of passive data offers a potential solution to creating reservoir-scale images in urban environments. A four-month, high station density passive seismic dataset collected in Long Beach, California is ideal for testing this hypothesis. Preliminary work on these data is promising. We clearly capture waveforms from earthquakes near (less than 15 km) and far (greater than 250 km). We successfully construct virtual sources through cross-correlation of low-frequency energy (0.175 to 1.75 Hz). The correlated energy is quite noisy and appears to be directed toward the northeast, suggesting that longer correlation times are needed for land data and that the Pacific Ocean is likely producing strong directed energy, respectively. Furthermore, the quality of correlation results differ depending on the time window. We argue that these differences are attributed to weather conditions, with records during stormier periods producing cleaner Green's functions than records during calmer periods.

INTRODUCTION

The Long Beach oil field is a productive oil field located below the city of Long Beach. Due to the urban environment, traditional techniques for collecting data for seismic imaging and velocity analysis are disruptive and difficult to perform. One alternative is using passive seismic data for this type of subsurface analysis. The effectiveness of such data for these purposes at the reservoir scale and in the urban environment is relatively unknown, but the recently deployed Long Beach seismic array provides a great opportunity to investigate their potential. The array is unique given its station density, recording period, and location. These parameters make this survey ideal for testing passive seismic imaging and tomography techniques from earthquake and exploration seismology.

Earthquakes oftentimes have source location depths on the order of kilometers, thereby producing waves that travel deep through the Earth's interior prior to reaching the surface. Depending on the amount of energy that a given event releases, the signal can be recorded by seismometers around the world. These two characteristics make data recorded from earthquakes ideal for resolving structures and velocities at the crustal/mantle scale, whether using body waves (Aki et al., 1977; Kissling, 1988; Romanowicz, 2008; Schmandt and Humphreys, 2010) or very low-frequency (less than

0.025 Hz) surface waves that can sample these depths (Yang and Ritzwoller, 2007; Tanimoto and Sheldrake, 2002). When dealing with these scales, what is considered dense station spacing can seem relatively sparse. For instance, USArray is a transportable array of 400 broad-band seismometers spaced 'densely' at approximately 500 km (Meltzer et al., 1999). With this denser Long Beach array, earthquake signal might be able to resolve structures and velocities at the reservoir scale.

A common drawback with using earthquake events for surface wave tomography is that surface wave dispersion is difficult to measure at frequencies higher than 0.05 Hz (Yang et al., 2008). Seismic interferometry with ambient noise can handle dispersion at these frequencies. By cross-correlating recordings of ambient seismic noise at two receivers, the traveltime between them can be recovered. This traveltime information can then be used for purposes such as velocity modeling, particularly when using low-frequency signal. Shapiro et al. (2005) and Lin et al. (2008) have been able to create velocity maps at the crustal scale by performing ambient noise cross-correlations on data recorded by USArray. At the reservoir scale, de Ridder and Dellinger (2011) showed that virtual low-frequency (0.35-1.75 Hz), omnidirectional Scholte waves along the ocean floor could be generated from ambient seismic noise. They were able to use the Scholte-wave traveltime information for tomographic imaging of structures in the near-surface (0-150 m).

In this report, we will show data that have been extracted from the Long Beach dataset. First, we will present snapshots of interpolated waveforms generated by earthquakes near and far. Second, we will present cross-correlation results for the same station location at various times of the survey. Both these results are viewed with an eye toward determining the capability of such an array for continuous reservoir monitoring in an urban environment using passive seismic data.

DATA

The Long Beach 3D seismic array was deployed by Nodal Seismic, Inc. for recording both passive and active seismic surveys. The array consists of about 2400 vertical-component geophones covering a region approximately 8.5 km north-south by 4 km east-west (Figure 1). Average station spacing is 330 m, both inline and crossline. While battery life limitations means stations are swapped out approximately every 8 days, station locations stay consistent throughout the survey. Data were being continuously recorded (24 hours/day) over a span of four months starting in January 2012, with a sampling rate of 500 Hz. This has provided us with approximately 48 TB of data. While the data have been low-cut at 3 Hz, there is still energy found in the suppressed lower frequencies.

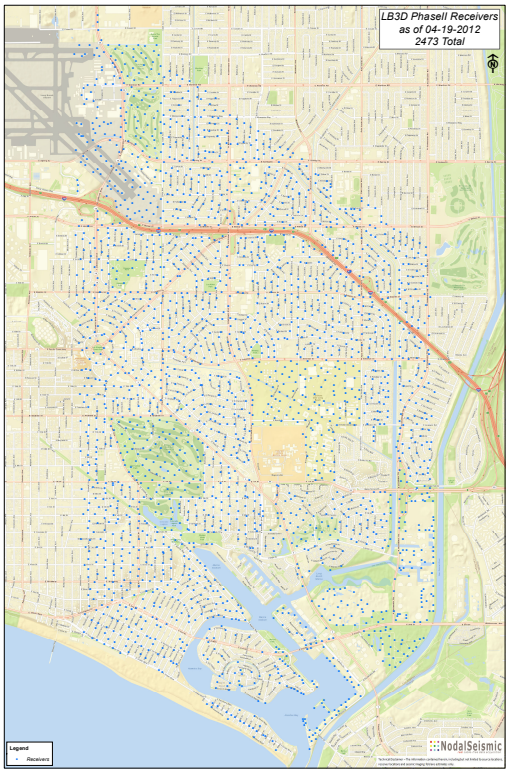

Figure 1: Map of receivers comprising the Long Beach 3D seismic array. [**NR**]

EARTHQUAKE RECORDINGS

With the San Andreas Fault running through California, the Long Beach survey picks up many events, both big and small. We present waveforms from a nearby (approximately 15 km east of the survey) M2.4 event in Yorba Linda, California, and a further away (approximately 250 km southeast of the survey) M4.9 event in Mexicali, Mexico. Given the spatial dimensions and duration of the Long Beach array, both events could potentially be used for resolving structures and velocities at the reservoir scale.

Interpolation

To create these snapshots, we implemented a normalized inverse distance weighting interpolation scheme. First, we normalized the amplitudes of the recordings because we did not want anomalously high amplitudes to dominate the interpolation results. Second, we created a 40 by 80 grid of rectangular cells that overlapped with the 8.5 km north-south by 4 km east-west region containing the array. To determine which stations would be used for interpolating the response at a given cell, we implemented nearest-neighbor binning.

Rather than average the recordings from each station for a given cell, we apply a weight to the relevant recordings for a given cell and then sum the recordings. The

weight is the normalized inverse of the distance between the location of the recording and the center of the cell, having the form

$$\mathbf{u}(\mathbf{x}) = \sum_{i=1}^{N} \frac{w_i(\mathbf{x})\mathbf{u}_i}{\sum_{i=1}^{N} w_i(\mathbf{x})}, \tag{1}$$

where

$$w_i(\mathbf{x}) = \frac{1}{d_i(\mathbf{x}, \mathbf{x}_i)}. \tag{2}$$

$\mathbf{u}(\mathbf{x})$ is the interpolated recording at cell $\mathbf{x}$, $w_i(\mathbf{x})$ is the weight applied to station i when interpolating for cell $\mathbf{x}$, $\mathbf{u}_i$ is the recording at station i, and $d_i(\mathbf{x}, \mathbf{x}_i)$ is the distance between the center of the cell $\mathbf{x}$ and the relevant station at location $\mathbf{x}_i$. This interpolation scheme weights recordings that are closer to the center of the cell more so than those recordings that are closer to the edges of the cell. The normalization of the weights by the sum of the weights ensures that the amplitudes from cell to cell are relatively similar, particularly because the amplitudes at each station were first normalized.

Earthquake Snapshots

Figure 2 displays an unfiltered snapshot from the relatively nearby Yorba Linda event, while Figure 3 displays the same snapshot after we applied a 8 Hz low-pass filter.

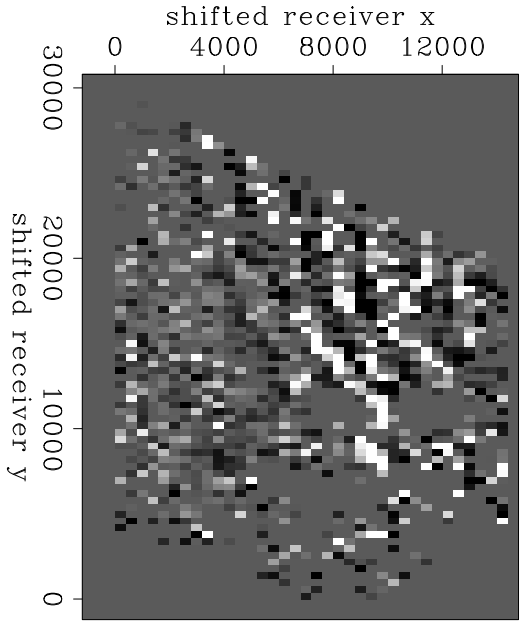

Figure 2: Snapshot of the interpolated waveform generated from the M2.4 Yorba Linda, CA event, roughly 15 km east of the Long Beach survey. [**CR**]

Figure 4 shows an unfiltered snapshot from the relatively far Mexicali event, while Figure 5 shows the same snapshot after we applied a 6 Hz low-pass filter.

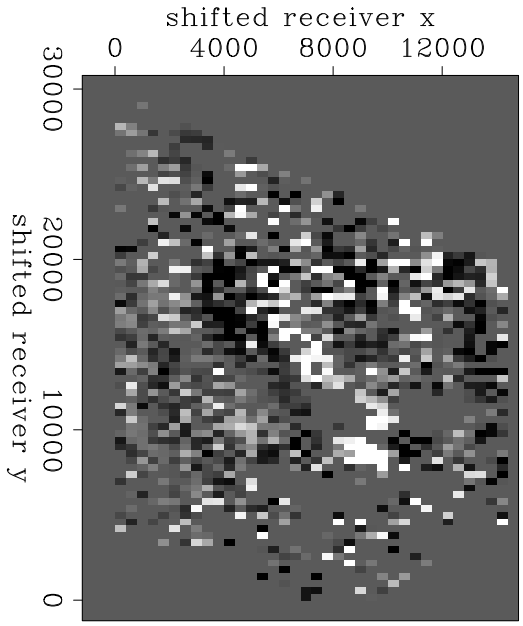

Figure 3: Same snapshot as Figure 2 but after applying a 8 Hz low-cut filter. [**CR**]

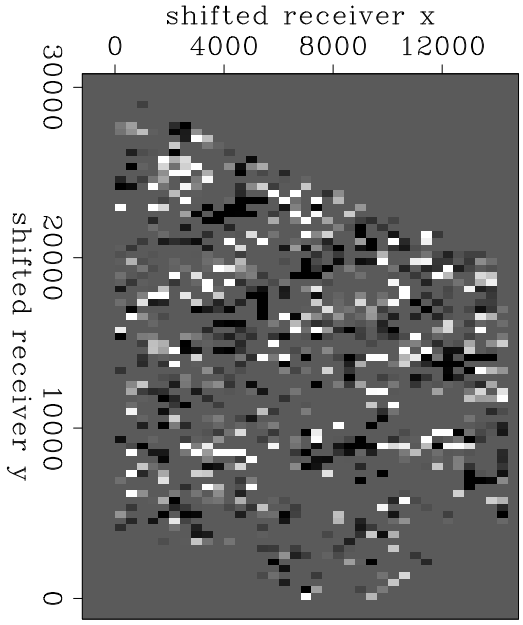

Figure 4: Snapshot of the interpolated waveform generated from the M4.9 Mexicali, Mexico event, roughly 250 km southeast of the survey. [**CR**]

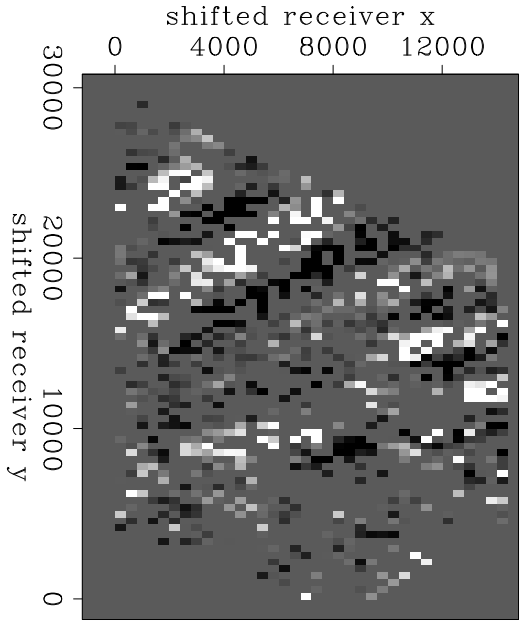

Figure 5: Same snapshot as Figure 4 but after applying a 6 Hz low-cut filter. [**CR**]

In both unfiltered snapshots (Figures 2 and 4), the incoming waveforms are distinguishable. However, when low-pass filtered (Figures 3 and 5) these waveforms are even easier to identify. This suggests that we are seeing surface waves (and perhaps S-waves), which are more prevalent at lower frequencies, rather than P-waves. Research by Yang and Ritzwoller (2007) and Tanimoto and Sheldrake (2002) have shown that surface waves can be used for resolving velocity structure at the crustal scale. With the denser station spacing of the Long Beach array, nearby and teleseismic events can potentially be useful for resolving structures and velocities at the reservoir scale.

SEISMIC INTERFEROMETRY AT LONG BEACH

Theory

In passive seismic interferometry, receivers record data from passive sources such as ambient seismic noise. Cross-correlating the two receiver recordings essentially turns the receivers into a source-receiver pair, thereby synthesizing new seismic responses. Specifically, cross-correlation recovers the Green's function, or the impulse response, and its time-reversed version between the two receivers, convolved with the autocorrelation of a source function such as noise (Wapenaar et al., 2010). In equation form

$$[G(x_B, x_A, t) + G(x_B, x_A, -t)] * S_N(t) = \langle u(x_B, t) * u(x_A, -t) \rangle \quad , \tag{3}$$

where G is the Green's function between two receiver locations (x_A, x_B), $S_N(t)$ is the autocorrelation of the source function (here it is noise), and u is the observed wavefield at a given receiver location. The result of cross-correlation is the traveltime difference of the recorded waves between the two given receivers.

A single cross-correlation of two recordings from two stations will likely produce noisy results. To improve signal-to-noise ratio, cross-correlations between multiple simultaneous recordings from two stations are stacked (or averaged) in the time-lag space (Curtis et al., 2006). This allows stationary signal phases to emerge, since these signals stack coherently and non-stationary phases stack incoherently. Therefore, stacking a month's worth of correlations should produce a better result than stacking a day's worth of correlations.

The method of passive seismic interferometry is effective only under certain conditions. The most important is that the principle of energy equipartition is satisfied. This means that noise must arrive at a receiver from all azimuths with the same amount of energy. If this is not satisfied, then correlation results may be far from ideal.

The station density and recording length of the array at Long Beach makes this dataset ideal for testing the limits of passive seismic interferometry in an urban environment. Higher station density provides more high-frequency information and should therefore provide better subsurface resolution. Longer recording times provide days to months of stacked correlations, as opposed to hours of stacked correlations. With longer stacked correlations, the convergence of the Green's function will improve and perhaps overcome the negative effects of cultural noise that is typically problematic in land data.

Method

Prior to performing any cross-correlations, we searched for time windows that were clear of significant seismic events. This is because one of the primary conditions for seismic interferometry to be effective is that the ambient seismic field satisfies the principle of equipartition. Because earthquakes produce high amounts of directed energy, they would potentially compromise our correlation results.

Once clear of major seismic events, we formed our time windows. We chose three windows spanning from 1: 30 pm, January 21 to 2: 00 am, January 22 (12.5 hours); 5: 00 pm, February 20 to 5: 00 am, February 21 (12 hours); and 2: 00 pm, February 27 to 4: 00 am, February 28 (14 hours). We received each data file as a time series for a single station, which meant that we had to re-sort our data according to recording time. We chose to synthesize 32.5-minute patches with 2.5-minute tapers at both ends, leading to a 2.5-minute overlap from one window in time to the next.

Prior to cross-correlating, we bandpass all the traces. de Ridder and Dellinger (2011) have had success generating virtual low-frequency (0.35-1.75 Hz), omnidirectional Scholte waves along the ocean floor, so we examine signals that have been similarly bandpassed between 0.175 Hz and 1.75 Hz. Because we want to compare correlation results over time, for each time window we cross-correlate all stations with the same station location. Finally, we stack each time patch within each time window to improve the signal-to-noise ratio of the correlations.

Results

All figures show correlation results with the same virtual source location and at the same acausal and causal time lags (−4 seconds and 4 seconds, respectively). Figure 6 and Figure 7 show the acausal and causal Green's functions from the 12.5 hours of correlations from January 21 to January 22. Figure 8 and Figure 9 show the acausal and causal Green's functions from the 12 hours of correlations from February 20 to February 21. Figure 10 and Figure 11 show the acausal and acausal Green's functions from the 14 hours of correlations from February 27 to February 28. Gaps in the array overlap with parts of the CSU Long Beach campus.

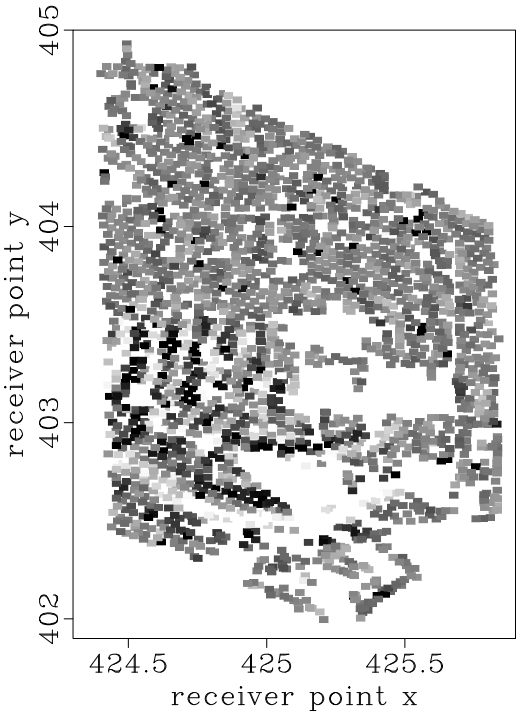

Figure 6: Snapshot of the Green's function at −4 second (acausal) time lag from the 12.5 hours of correlations from January 21 to January 22. [**CR**]

Discussion

A common observation is that the correlation energy is strongest in the southwest portion of the array at acausal (negative) time lags and strongest in the northeast portion of the array at causal (positive) time lags. This might be a consequence of the location of the array. Based on results from research utilizing data from ocean-bottom cables, the correlating energy is typically symmetric and circular about the virtual source location at both causal and acausal times. This is because energy typically reaches a given receiver in equal amounts from all azimuths in these deep-water environments, where the primary source of seismic energy is generated from the interaction of ocean currents with the ocean bottom. In other words, the principle of energy equipartition is more or less satisfied in deep-water environments. However, these results from Long Beach suggest that this principle is not being satisfied. The

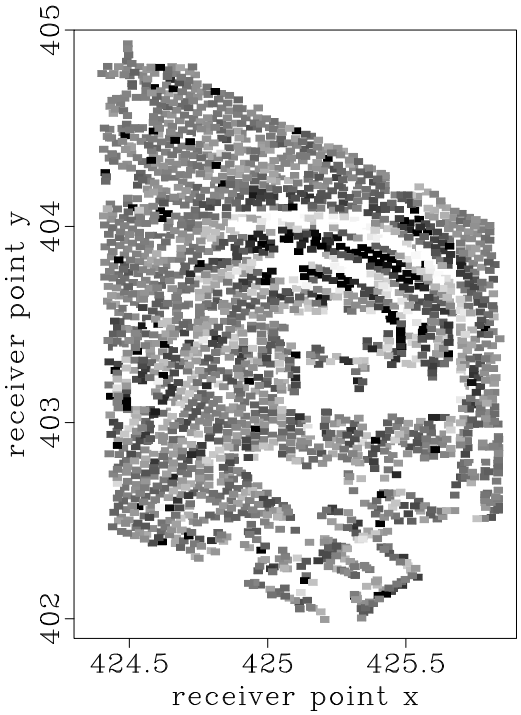

Figure 7: Snapshot of the Green's function at 4 second (causal) time lag from the 12.5 hours of correlations from January 21 to January 22. [**CR**]

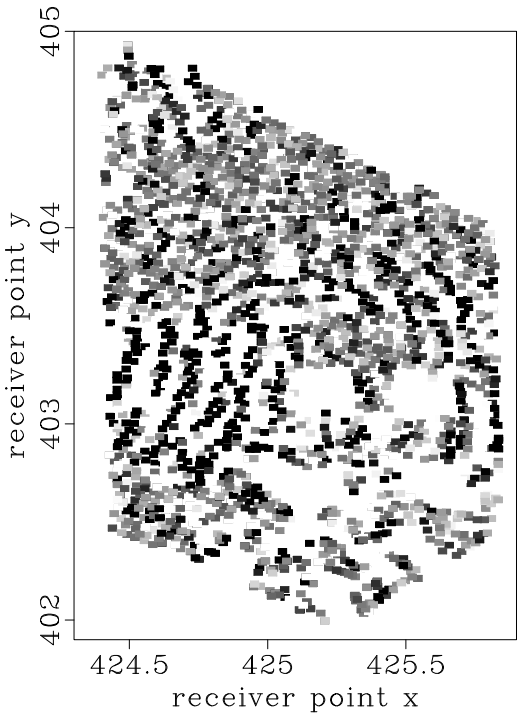

Figure 8: Snapshot of the Green's function at -4 second (acausal) time lag from the 12 hours of correlations from February 20 to February 21. [**CR**]

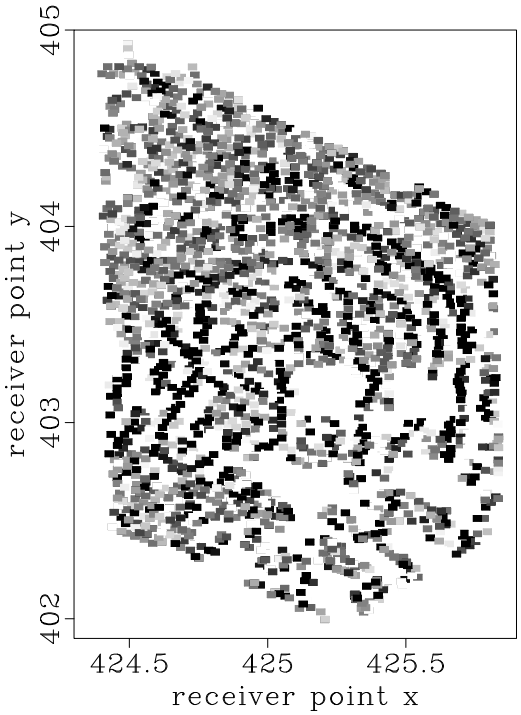

Figure 9: Snapshot of the Green's function at 4 second (causal) time lag from the 12 hours of correlations from February 20 to February 21. [**CR**]

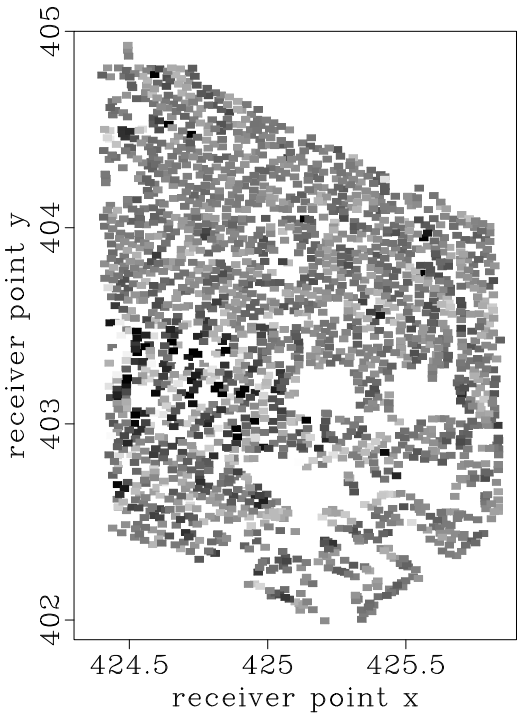

Figure 10: Snapshot of the Green's function at -4 second (acausal) time lag from the 14 hours of correlations from February 27 to February 28. [**ER**]

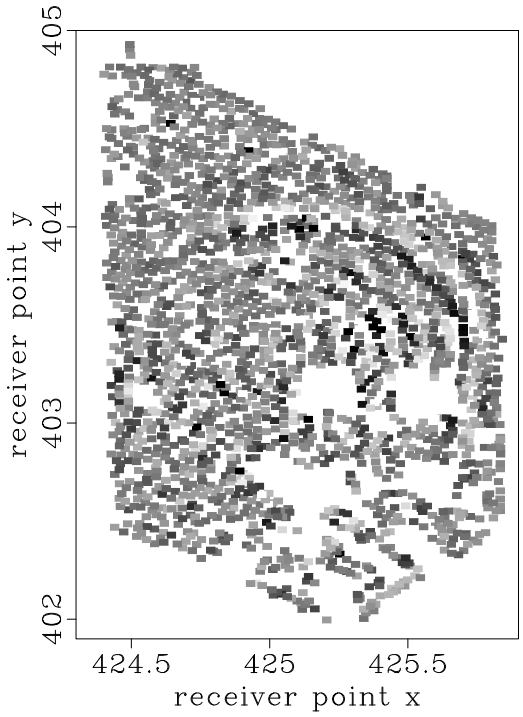

Figure 11: Snapshot of the Green's function at 4 second (causal) time lag from the 14 hours of correlations from February 27 to February 28. [**ER**]

directionality of the Green's function from southwest to northeast suggests that the Pacific Ocean (which is south-southwest of the array) is a large source of directed, low-frequency energy. This causes the Green's function at causal and acausal times to be asymmetric.

The primary difference between the Green's function from each time window is the quality. The correlation energy from the January window is by far the most distinct, followed by the result from late-February and the result from mid-February. A look at the weather conditions in southern California may explain these results. At the time of the January time window, there was a large rainstorm that hit the region (http://www.wrh.noaa.gov/). During the late-February window, conditions were somewhat windy. In mid-February, conditions were pretty mild. Therefore, it appears that correlation results are best during stormy conditions, which happens to also be the case with seismic interferometry results from ocean-bottom cable data (de Ridder and Dellinger, 2011). These conditions may be best because during a storm the energy generated by the Pacific Ocean is much higher relative to any other noise source. Because the ocean is likely the dominant source of the directed, low-frequency energy that we see, then the more relative energy it has, the cleaner the resulting Green's function will be. With more correlation time, the results from February may be able to match the result from January.

FUTURE WORK

Earthquake waveforms and cross-correlation results are promising enough that the next step is to perform surface wave tomography for various time windows. For reservoir monitoring, using surface waves generated by passive seismic interferometry appears to be a better option than using surface waves generated by earthquakes. We are interested in the relatively higher frequencies, which seismic interferometry and ambient noise tomography is better equipped to handle. Passive seismic interferometry is also better for reservoir monitoring because signal is continuously available and is not dependent on random events like earthquakes. Therefore, time-lapse images at the reservoir scale may be possible with passive seismic interferometry.

CONCLUSION

Because it is an urban environment, the city of Long Beach is a suitable location to investigate the use of passive seismic data for subsurface imaging and velocity analysis at the reservoir scale. The dense, continuously recording Long Beach array is ideal for time-lapse analysis. We captured a variety of earthquake waveforms, generated both near to and far from the array, that could be used for tomographic imaging. We have also captured correlating energy at low frequencies using seismic interferometry techniques, which can also be used for tomographic imaging. Therefore, there are indications that seismic land data from an urban environment has the potential to be used for subsurface monitoring.

ACKNOWLEDGMENTS

We gratefully acknowledge Signal Hill Petroleum, Inc. for access to this dataset and permission to publish. We would particularly like to thank Dan Hollis for both his effort in helping us acquire this dataset and his enthusiasm in sharing these data with us.

REFERENCES

Aki, K., A. Christoffersson, and E. Husebye, 1977, Determination of the three-dimensional seismic structure of the lithosphere: Journal of Geophysical Research, **82**, 277–296.

Curtis, A., P. Gerstoft, H. Sato, R. Snieder, and K. Wapenaar, 2006, Seismic interferometry - turning noise into signal: The Leading Edge, **25**.

de Ridder, S. and J. Dellinger, 2011, Ambient seismic noise eikonal tomography for near-surface imaging at Valhall: The Leading Edge, **30**, 506–512.

Kissling, E., 1988, Geotomography with local earthquake data: **26**, 659–698.

Lin, F., M. Moschetti, and M. Ritzwoller, 2008, Surface wave tomography of the western United States from ambient seismic noise: Rayleigh and Love wave phase velocity maps: Geophysical Journal International, **173**, 281–298.

Meltzer, A., R. Rudnick, P. Zeitler, A. Levander, G. Humphreys, K. Karlstrom, G. Ekstrom, R. Carlson, T. Dixon, M. Gurnis, P. Shearer, and R. van der Hilst, 1999, USArray initiative: Geological Society of America TODAY, **9**, 8–10.

Romanowicz, B., 2008, Using seismic waves to image Earth's internal structure: Nature, **451**, 266–268.

Schmandt, B. and E. Humphreys, 2010, Complex subduction and small-scale convection revealed by body-wave tomography of the western United States upper mantle: Earth and Planetary Science Letters, **297**, 435–445.

Shapiro, N., M. Campillo, S. L., and M. Ritzwoller, 2005, High-resolution surface-wave tomography from ambient seismic noise: Science, **307**, 1615–1618.

Tanimoto, T. and K. Sheldrake, 2002, Three-dimensional S-wave velocity structure in southern California: Geophysical Research Letters, **29(8)**.

Wapenaar, K., D. Draganov, R. Snieder, X. Campman, and A. Verdel, 2010, Tutorial on seismic interferometry: Part 1—Basic principles and applications: Geophysics, **75**, 75A195–75A209.

Yang, Y. and M. Ritzwoller, 2007, Teleseismic surface wave tomography in the western U.S. using the transportable array component of usarray: Geophysical Research Letters, **35**, 1–5.

Yang, Y., M. Ritzwoller, F. Lin, M. Moschetti, and N. Shapiro, 2008, Structure of the crust in uppermost mantle beneath the western United States revealed by amibent noise and earthquake tomography: Journal of Geophysical Research, **113**, 1–9.